Materials Science and Engineering A 2010, 572, 1126-1134

Modeling of Continuous Dynamic Recrystallization in Commercial-Purity Aluminum

Håkan Hallberg*, Mathias Wallin, Matti Ristinmaa

Division of Solid Mechanics
Lund University, Box 118, S-221 00 Lund, Sweden
*hakan.hallberg@solid.lth.se

Abstract

A constitutive model for polycrystalline metals is established within a micromechanical framework. The inelastic deformation is defined by the formation and annihilation of dislocations together with grain refinement due to continuous dynamic recrystallization. The recrystallization studied here occurs due to plastic deformation without the aid of elevated temperatures. The grain refinement also influences the evolution of the dislocation density since the recrystallization introduces a dynamic recovery as well as additional grain and subgrain boundaries, hindering the movement of dislocations through the material microstructure. In addition, motivated by experimental evidence, the rate dependence of the material is allowed to depend on the grain size. Introducing a varying grain size into the evolution of the dislocation density and in the rate dependence of the plastic deformation are believed to be important and novel features of the present model. The proposed constitutive model is implemented in a numerical scheme allowing calibration against experimental results, which is shown using commercial-purity aluminum as example material. The model is also employed in macroscale simulations of grain refinement in this material during extensive inelastic deformation.

Keywords: Recrystallization, Viscoplasticity, ECAP, Equal channel angular pressing, Aluminum, AA1050

DOI: 10.1016/j.msea.2009.09.043

1 Introduction

During the last two decades there has been an increasing trend to incorporate more explicit influence of micromechanical material processes as constitutive models are gradually refined, taking additional metallurgical knowledge into account. Macroscopic models of plasticity and viscoplasticity can in this way be formulated based on e.g. micromechanical descriptions of dislocation dynamics. This bridging of scales allows models that maintain the computational efficiency of macroscopic phenomenological models while incorporating a material description that is closer to the actual metallurgical processes on the microscale. By this micromechanical approach, material effects of dislocation generation, interaction and annihilation can be combined with the influence of grain boundaries, changes in grain size and material annealing through recrystallization.

The recrystallization process is driven by a strive to lower the energy stored within the material microstructure. This occurs through the formation of new grains of relatively lower internal dislocation density. Dislocations are, however, also to a great extent pinned at the extensively expanded grain boundary area as subgrains are formed and as the grains are refined. The effect is a second-stage hardening of the material due to dislocation immobilization and storage.

Incorporating recrystallization into the model thus allows an attractive addition to the traditional macroscopic simulation models. Not least since grain refinement is an important process parameter in e.g. industrial metal forming. Grain refinement has also gained increasing interest in relation to processes such as friction stir welding, where the grain size strongly influences the properties of the welded joint. Knowledge of the grain size thus allows better understanding of both hardness and ductility in the material being deformed and, perhaps more importantly, improved control over the final product.

The micromechanical kinetics of grain refinement in aluminum exposed to severe plastic deformation has long been a matter of discussion. In recent years there seem, however, to be some consensus that the dynamic recrystallization in aluminum can be ascribed to three processes, e.g. [1, 2, 3, 4]. These processes are: (1) Discontinuous dynamic recrystallization (DDRX), which is the historically most investigated process, involving nucleation of grain embryos and subsequent grain growth. (2) Continuous dynamic recrystallization (CDRX), where dislocation networks form subgrain structures with low-angle boundaries. As plastic deformation then progresses, the misorientation increases and eventually grain formation may occur as the initially mobile grain boundaries are immobilized through e.g. Zener pinning. (3) Geometric dynamic recrystallization (GDRX), where the initial grains are deformed and eventually fragmented as high-angle boundaries created by subgrain formation are pinched-off and annihilated.

The process of dynamic recrystallization in aluminum during cold deformation is still not fully understood, cf. [4, 5]. There exists, however, a vast amount of information –

sometimes partially conflicting – regarding the corresponding process at elevated temperatures, information which of course pertain largely also to cold deformation processes. In this respect it can be noted that in fcc materials of high stacking-fault energy such as high-purity aluminum, DDRX is generally believed to be restricted by dynamic recovery through e.g. cross-slip. Instead, CDRX operates to give the observed microstructure. Some authors, however, report that DDRX indeed may occur in high-purity aluminum at elevated temperatures and under conditions described by certain intervals of the value of the Zener-Hollomon parameter, cf. [6]. In some cases DDRX is observed to work in combination with CDRX and even by CDRX being a nucleation source for DDRX, [7, 8]. Yet other sources report GDRX to be the dominating grain refinement mechanism, e.g. [2]. In general it seems, however, that grain refinement due to DDRX in aluminum is restricted by the presence of impurities and grain refinement in commercial-purity aluminum is believed to be dominated by CDRX, e.g. [1, 4, 7].

Constitutive models for DDRX-based grain refinement are frequent in the published literature, these models are mainly based on explicit expressions for the grain size as a function of plastic deformation. Material models of CDRX processes are more scarce, however. An example is given in [9] where the recrystallization process is formulated by quantifying the occurrence of low-angle boundaries and their transition into high-angle boundaries with progressing deformation. In the present formulation, the grain size is taken as a function of the accumulated viscoplastic strain and the microstructural misorientation is assumed to be related to the magnitude of this deformation measure. A threshold value of the accumulated viscoplastic strain is assumed to correspond to the conditions where new grains begin to form within immobilized subgrain boundaries.

Influential work on constitutive modeling of crystalline materials by means of dislocation dynamics was performed already in [10, 11] where it was concluded that sound material descriptions could be established through micromechanical reasoning. These formulations have been followed by numerous models where additional aspects of dislocation dynamics are incorporated. Recent constitutive models based on micromechanics are given in e.g. [12, 13]. Although such models – based on dislocation density evolution laws and considering recrystallization – have been proposed by e.g. [13], the present model gives a coherent formulation suitable for large-scale simulations of materials undergoing continuous dynamic recrystallization. In addition, the present model includes novel features in terms of allowing the average grain size to influence both the evolution of the dislocation density and also the rate-dependence of the material. The latter characteristic has, for example, been observed in nickel by [14], in gold by [15] and in aluminum by [16, 17], this being the material under consideration in the present work. However motivated by experimental evidence, previous models, such as in [18], has to the authors' knowledge treated the grain size as a constant parameter rather than a variable, if considered at all.

The introduction of the grain size in the evolution law for the dislocation density is motivated by the dynamic recovery that occur due to migration and subsequent immobilization of high-angle subgrain boundaries, creating new grains of low dislocation density, cf. [19, 20]. In addition, the grain refinement also introduces a significant increase in grain boundary area which hinders the movement of glissile dislocations. The obstacles to dislocation mobility posed by the grain boundaries – and the concentration of dislocations into subgrain structures – cause additional hardening of the material as the recrystallization progresses. The reduced mobility of dislocations in aluminum due to reduced grain size is discussed by for example [21].

The present paper proposes a constitutive model for macroscale simulations of metals and steel, based on the micromechanical processes of dislocation dynamics and grain refinement through continuous dynamic recrystallization. On this micromechanical basis, a model describing finite strain viscoplasticity is established. The model is then applied to a commercial-purity aluminum, exposed to severe plastic deformations where recrystallization occurs in the cold state, i.e. without additional influence of elevated temperature.

The paper is divided into sections, whereof the first concerns the micromechanical processes of grain refinement and the evolution of dislocation density and the influence of these processes on the flow strength of the material. Next, the necessary components of finite-strain viscoplasticity are described together with the evolution of the macroscopic plastic deformation. This is followed by some illustrative numerical simulations. Some concluding remarks close the paper.

2 Micromechanical considerations

The plastic behavior of metals is mainly due to the presence of lattice defects, i.e. the ability for dislocation generation and propagation in the material. Although models that account for individual dislocation exist they are, due to the high computational effort required, not suitable for large scale simulations. To be able to perform large scale simulations on engineering structures, quantities that represents their averaged microstructural counterparts must be defined. In the present work use will be made of the dislocation density and the average grain size as variables representing the microstructure. The evolution of these variables and their influence on the macroscopic deformation hardening of the material will be discussed in the next two sub-sections. But as much of the experimental data is obtained by use of ECAP processing, this method will be briefly recaptured before proceeding to the descriptions of dislocation density and grain refinement. Since introduced in 1981 by Segal [22], ECAP has become a widely used method for producing very fine-grained materials through extensive plastic deformation, cf. also [23, 24]. A typical ECAP-setup is shown in Fig. 1 where also the corner angle Ψ and the channel angle Φ are defined. Following [25], the effective plastic strain, $\varepsilon_{\text{eff}}^{\text{vp}}$, imposed on the workpiece that has passed through the

ECAP die can be calculated as

$$\varepsilon_{\text{eff}}^{\text{vp}} = \frac{N_{\text{pass}}}{\sqrt{3}} \left[2\cot\left(\frac{\Phi}{2} + \frac{\Psi}{2}\right) + \Psi \operatorname{cosec}\left(\frac{\Phi}{2} + \frac{\Psi}{2}\right) \right] \tag{1}$$

where N_{pass} is the number of passes through the die. Expression (1) has been used to quantify the deformation in several studies on fine-grained materials produced by ECAP, e.g. in [26, 27, 28]. With a channel angle $\Phi = 90°$, one ECAP-pass imposes a strain of $\varepsilon_{\text{eff}}^{\text{vp}} \approx 1$ in the workpiece material, with only a minor dependence on the angle Ψ. Different deformation modes can be obtained if the workpiece is rotated around its length axis in between each pass. Depending on the rotation (90°,180°, rotation in different directions etc.) different process routes denoted by letters have become standardized, cf. [24]. In the present work the constitutive model is calibrated to comply with commercial-

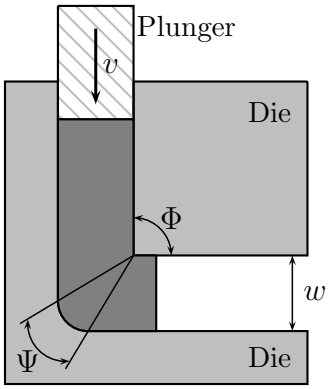

Figure 1: Schematic illustration of the ECAP process.

purity aluminum which is a fcc-structured material, known to undergo continuous dynamic recrystallization at room temperature. Moreover, much material data regarding aluminum is available in the literature.

2.1 Evolution of grain size

The creation of new grains, of relatively low dislocation density, through recrystallization is driven by a strive to lower the stored energy of deformation, i.e. the accumulated dislocation density in the material. Recrystallization occurs in the deformed material through the formation and migration of high-angle grain boundaries, that constitute a distinct interface between the previously deformed material and the new fine-grained structure. The expanding grain boundary area hinders the movement of the dislocations and pins them at the boundaries, thereby increasing the yield stress of the material. As discussed in the introductory section, the present model considers aluminum of commercial-grade purity and thus focuses on grain refinement due to continuous dynamic recrystallization (CDRX), cf.

[1, 2, 9]. At lower levels of strain, dislocations starts to get pinned at existing grain boundaries but they also become entangled in subgrain structures within the present grains. As the plastic deformation increases, dislocations are accumulated in the initially low-angle boundaries of the subgrains. Through this dislocation accumulation, the misorientation is increased and eventually high-angle boundaries are formed. The migration of these high-angle boundaries may be hindered as they are pinned down by e.g. particle inclusions and with progressing plastic deformation, the pinned subgrain boundaries get pinched-off, resulting in the formation of new grains from the subgrain structures. The material microstructure exposed to CDRX will in this way consist of deforming pre-existing grains, evolving subgrains and grains newly created from such subgrains. The final recrystallized microstructure contains grains and subgrains of nearly the same size, cf. [7].

The process of subgrain formation, dislocation accumulation, increase of misorientation and eventually formation of new grains is of course a continuous and gradual process. In the present model a critical plastic deformation level $\varepsilon_{\mathrm{c}}^{\mathrm{vp}}$ is assumed to correspond to the critical stage of this process, where enough misorientation to induce grain formation is reached. This parameter will then describe the incubation period before recrystallization sets in, i.e. the time during which e.g. subgrain growth and subgrain boundary pinning occurs.

Both recrystallization and grain growth are processes that take place in the material microstructure. While the former process leads to increased hardening as the grains are refined, e.g. as described by the Hall-Petch relation, and as dislocations are pinned at the expanding grain boundaries, the latter process induce a softening of the material through increased ductility. Further grain size changes such as through secondary recrystallization and grain growth are not considered here. These matters are extensively discussed by e.g. [19, 29]. The present model is focused on continuous dynamic recrystallization, leading to a grain refinement in the material whereby the average grain diameter D will be gradually reduced from an initial value D_0. If the recrystallization process is allowed to proceed until the entire microstructure is recrystallized, the average grain diameter will approach a constant steady-state value D_{f}, cf. [30, 31, 32]. Several studies have identified this grain size as being related to the Zener-Hollomon parameter, representing a temperature-compensated strain rate, cf. [33, 34]. Since an isothermal formulation is adopted here, the Zener-Hollomon parameter will only constitute a constant scaling of the strain rate, allowing the final grain size to be taken as a constant parameter in the present model.

The initial grain size D_0 will be gradually refined once the effective plastic deformation reaches the critical deformation level $\varepsilon_{\mathrm{c}}^{\mathrm{vp}}$. In the present model the grain size is taken to be exponentially decreasing with effective plastic strain. This format is experimentally motivated in Table 1, where the grain size for different levels of plastic deformation is shown for a set of various aluminum grades. In Table 1 use is made of (1) to obtain the plastic strain for different numbers of ECAP passes and different channel angles. The relative

stability of the grain size at large plastic strains gives additional substantiation in taking D_f as a constant parameter. To ensure a smooth transition of the microstructure from the

Table 1: Recrystallized grain size D, stated in μm, in different aluminum grades as function of plastic strain. The data is compiled from various sources.

$\varepsilon_{\mathrm{eff}}^{\mathrm{vp}}$	AA1200 [35]	Al 5N [28]	5083 Al [36]	Al3Mg [37]	AA1050 [38]
0	41.48	280	200	250	100
1	3.83	120	0.55	–	–
2	2.82	82	–	–	–
3	2.22	77	–	–	–
4	2.22	–	0.3	–	–
5	2.42	–	–	–	–
5.6	–	–	–	0.25	–
6	2.01	–	–	–	–
7	–	–	–	–	–
8	–	–	0.3	–	1.2

initial grain size D_0 into the saturation grain size D_f, the average grain size in the present work is described by

$$D = D_0 - (D_0 - D_\mathrm{f}) \left[1 - \exp\left(-k_\mathrm{X} \left\langle \widetilde{\varepsilon}_{\mathrm{eff}}^{\mathrm{vp}} - \varepsilon_\mathrm{c}^{\mathrm{vp}} \right\rangle^{c_\mathrm{X}}\right)\right], \qquad D_\mathrm{f} \leq D \leq D_0 \tag{2}$$

where k_X and c_X are parameters that define how fast the recrystallization proceed with increasing plastic deformation. The McCauley brackets $\langle\cdot\rangle$ indicate that no recrystallization will occur until the strain satisfies $\widetilde{\varepsilon}_{\mathrm{eff}}^{\mathrm{vp}} > \varepsilon_\mathrm{c}^{\mathrm{vp}}$. In the present model this critical strain – where CDRX start to appear – is set as $\varepsilon_\mathrm{c}^{\mathrm{vp}} = 0.1$ which will give the grain size evolutions shown in Fig. 2, consistent with the experimental data compiled in Table 1. It can be noted that by considering a commercial-purity aluminum, the migration of subgrain boundaries is more restricted than in high-purity aluminum due to the additional presence of impurities and the rate of recovery is therefore slower, cf. [16]. These mechanisms assist in the formation of a fine grained microstructure through CDRX.

Although grain refinement has been observed in aluminum under uniaxial compression at elevated temperature, e.g. [1], other authors report grain refinement to be limited or absent in the case of pure uniaxial loading at room temperature which is the situation considered here, cf. [39]. In order to allow the present model to – optionally – capture such deformation mode dependence, the modified effective viscoplastic strain quantity $\widetilde{\varepsilon}_{\mathrm{eff}}^{\mathrm{vp}}$ was introduced in expression (2). The evolution of this quantity is here taken as

$$\dot{\widetilde{\varepsilon}}_{\mathrm{eff}}^{\mathrm{vp}} = \left[1 - a\cos^2(3\theta)\right] \dot{\varepsilon}_{\mathrm{eff}}^{\mathrm{vp}}, \quad \theta = \frac{1}{3}\arccos\left(\frac{3\sqrt{3}}{2}\frac{J_3}{J_2^{3/2}}\right) \tag{3}$$

where $\dot{\varepsilon}_{\text{eff}}^{\text{vp}}$ is the effective viscoplastic strain rate. The Lode angle, θ, is defined by the second and third invariants of the deviatoric Kirchhoff stress tensor, $\boldsymbol{\tau}^{\text{dev}}$, which are denoted by J_2 and J_3, respectively, cf. [40]. Note that the parameter $a \in [0, 1]$ allows control of the extent of recrystallization during uniaxial loading. This parameter is in the present case set to $a = 1$ whereby the grain size will be held constant in the cases of purely uniaxial tension and compression, i.e. for $\theta = 0°$ and $\theta = 60°$. It should also be noted that by setting $a = 0$, no restriction on the recrystallization is posed by the deformation mode.

In Fig. 2, expression (2) is fitted to experimental results from a number of sources. Note that these fits are based on the assumption that the plastic deformation is homogeneous and that plasticity is due to pure shear, i.e. the Lode angle, $\theta = 30°$ which implies that $\varepsilon_{\text{eff}}^{\text{vp}} = \tilde{\varepsilon}_{\text{eff}}^{\text{vp}}$. Small elastic strains are assumed. The model response shown in Fig. 2 is obtained using the parameter values $k_{\text{X}} = 3.8$ and $c_{\text{X}} = 2$. In the numerical simulations

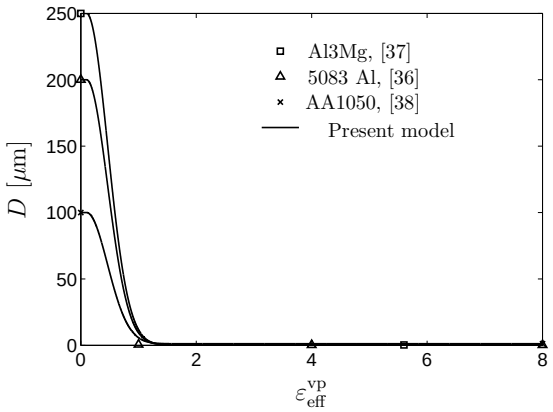

Figure 2: Grain size as function of plastic deformation for various aluminum grades. The present model (solid lines) calibrated against experimental results (symbols).

presented in next section the initial and final grain size are taken as $D_0 = 100$ μm and $D_{\text{f}} = 1$ μm, respectively. These values are representative for commercial-purity aluminum, cf. Table 1.

2.2 Flow strength mechanisms and evolution of dislocation density

The threshold for plastic deformation is on the macroscopic level manifested by the yield stress. Once a metallic material is deformed beyond it's yield stress, any further – now inelastic – deformation is controlled by the creation, activation, movement and annihilation of dislocations. In fact, the movement of dislocations is the dominant feature of inelastic deformation when considering levels of temperature and strain rate where creep and diffusion are not significant. During plastic flow the motion of dislocations is hindered by either short- or long-range barriers. The short-range obstacles consist of the Peierls' stress needed to overcome lattice friction, point defects such as vacancies and interstitials, other

dislocations intersecting the current slip plane, solute atoms and alloying elements. Long-range obstacles include grain boundaries and far-field forest dislocations. The short-range barriers are thermally activated, i.e. they are overcome by a change in thermal energy, while the stronger long-range obstacles are independent of temperature.

As discussed previously, the recrystallizing microstructure will contain a conglomerate of pre-existing grains, newly formed grains and evolving subgrains. The expanding boundaries of grains and subgrains act as obstacles to dislocation motion and the mobility of dislocations will thus be progressively reduced with increasing volume fraction of grain boundaries. Taking the grain size D as an average of the grain and subgrain sizes in the current microstructure – also noting that the grains and subgrains after CDRX are of approximately the same size, cf. [7] – it is assumed that the yield stress is inversely proportional to the square root of the grain size. This allows the celebrated Hall-Petch relation to be recovered as

$$\sigma_{\mathrm{y}} \propto D^{-1/2} \tag{4}$$

The validity of the Hall-Petch relation is confirmed for aluminum over a wide range of grain sizes in [42, 43, 44].

As suggested by G. I. Taylor already in 1934, the mobility of dislocations – and thereby also the progression of plastic flow – will become increasingly restricted as dislocations are multiplied, entangled and interlocked. These processes result in a macroscopic deformation hardening of the material. The macroscopic yield stress is commonly modeled as being proportional to the square root of the dislocation density, e.g. [11, 18, 32, 45], i.e. to $\sqrt{\rho_{\mathrm{d}}}$, This results in a second term, adding to the flow strength of the material according to

$$\sigma_{\mathrm{y}} \propto \sqrt{\rho_{\mathrm{d}}} \tag{5}$$

Combining (4) and (5) the following format for the yield stress is obtained

$$\sigma_{\mathrm{y}}\left(\rho_{\mathrm{d}}, D\right) = \sigma_{\mathrm{y0}} + H\left(\sqrt{\frac{\rho_{\mathrm{d}}}{\rho_{\mathrm{d}}^{0}}} - 1\right) + k_{\mathrm{D}}\left(\sqrt{\frac{D_0}{D}} - 1\right) \tag{6}$$

where k_{D} is a stress intensity factor and σ_{y0} the Peierls' stress needed to overcome lattice friction. This stress can be viewed as the yield stress for the virgin material, i.e. $\sigma_{\mathrm{y0}} = \sigma_{\mathrm{y}}\left(\rho_{\mathrm{d}}^{0}, D_0\right)$. Note that ρ_{d}^{0} is introduced in (6) to denote the initial density of dislocations in the material. The hardening modulus H corresponds to a generalized Taylor factor, comparable to what has been utilized in numerous models, e.g. in [11, 18, 32, 45].

Several proposals have been given regarding dislocation density evolution laws. Following the works of [10, 11], the evolution of dislocation density is commonly described on differential form, relating it to the plastic deformation. The total accumulated dislocation

density ρ_{d} – corresponding to the stored energy of cold work – is here described through an evolution law, put forward in e.g. [18, 45], on differential form as

$$\dot{\rho}_{\mathrm{d}} = \left(\bar{d}_1\sqrt{\rho_{\mathrm{d}}} - \bar{d}_2\rho_{\mathrm{d}}\right)\dot{\varepsilon}_{\mathrm{eff}}^{\mathrm{vp}} \tag{7}$$

where $\bar{d}_{1,2}$ are parameters related to the microstructural behavior of the material. The multiplication of dislocations through e.g. Frank-Read mechanisms is dictated by $\bar{d}_1$ and dynamic recovery through e.g. cross-slip by $\bar{d}_2$.

Once recrystallization is initiated in the material the corresponding microstructural changes will influence the dislocation dynamics. As the average grain size decreases, the volume fraction of grain boundary area will increase. The grain boundaries act as barriers against the movement of mobile dislocations, pinning them at the boundaries. In addition, the new grains that are formed will be of considerably lower dislocation density as the recrystallization process strives to lower the energy stored within the material. Effectively the refined grain size will lead to a second-stage hardening of the material due to the substantial dislocation storage at the increasing number of grain and subgrain boundaries, cf. [18, 46]. From this reasoning, the effects of recrystallization will appear as an additional term in the evolution law for the dislocation density. Adding this quantity to the dislocation density evolution law (7), and normalizing by the initial dislocation density ρ_{d}^0, gives the new format

$$\frac{\dot{\rho}_{\mathrm{d}}}{\rho_{\mathrm{d}}^0} = \left[d_1\sqrt{\frac{\rho_{\mathrm{d}}}{\rho_{\mathrm{d}}^0}} - d_2\frac{\rho_{\mathrm{d}}}{\rho_{\mathrm{d}}^0} + d_3\frac{D_0}{D}\right]\dot{\varepsilon}_{\mathrm{eff}}^{\mathrm{vp}} \tag{8}$$

The mobility of dislocations is in part controlled by the available mean free path for dislocation movement. If both the distance between the dislocations themselves and also to the obstacles posed by grain boundaries are considered, the available distance between dislocations will be proportional to $1/D + \sqrt{\rho_{\mathrm{d}}}$. With the $\sqrt{\rho_{\mathrm{d}}}$-proportional term covered by the d_1 parameter, this motivates the format of the third term, dependent on D, in (8), where d_3 is a parameter that determines the influence of grain size – and thereby also indirectly of recrystallization – on the dislocation density evolution. The expression of this grain size dependent term has a format similar to that used in [18, 47, 46].

To calibrate the yield stress and dislocation density evolution use will be made of the experimental data on AA1050 aluminum presented by [38], as shown in Fig. 3. The experimental data is obtained from ECAP-processed AA1050 which is subsequently subjected to compression tests. For calibration purposes it is assumed that the deformation process is slow, i.e. no viscous effects are considered. Moreover, idealized conditions are assumed, where each ECAP pass results in the effective plastic strain 1 and the deformation mode is pure shear. The assumption of a homogeneous cross section is in close approximation to the true response for the interior of the specimen. At the surfaces close to the tool significant deviations from this assumption can occur. The matter of inhomogeneity will

be discussed in relation to the numerical simulations. The assumption of a homogeneous cross section results in that the evolution laws (8), (3) together with (2) and (6) can be integrated without considering the boundary value problem.

Based on the experimental data in Fig. 3, the Hall-Petch component of the yield stress is calibrated by setting $k_{\mathrm{D}} = 6.8$ MPa, a value which is of the same order of magnitude as that found for high-purity aluminum in [42]. The data shown in Fig. 3 also allows calibration of the Peierls-stress $\sigma_{\mathrm{y0}} = 48.6$ MPa and the hardening modulus $H = 0.7$ MPa, found in equation (6). The initial density of dislocations is set to $\rho_{\mathrm{d}}^0 = 8 \times 10^9$ m^{-2} in parity with what is used in [48] for aluminum. For the calibration, the initial values used to obtain the fitting in Fig. 3 are: No ECAP $(D, \rho_{\mathrm{d}}/\rho_{\mathrm{d}}^0) = (100\ \mu\mathrm{m}, 1)$, 1 ECAP pass $(D, \rho_{\mathrm{d}}/\rho_{\mathrm{d}}^0) = (5.75\ \mu\mathrm{m}, 8.3 \times 10^3)$, and 8 ECAP passes $(D, \rho_{\mathrm{d}}/\rho_{\mathrm{d}}^0) = (1.2\ \mu\mathrm{m}, 8.7 \times 10^3)$. These values are also in line with what is obtained from the finite element simulations, cf. Fig. 5. The calibration results in the constitutive parameters $d_1 = 715.54$, $d_2 = 7.7$ and $d_3 = 437.5$.

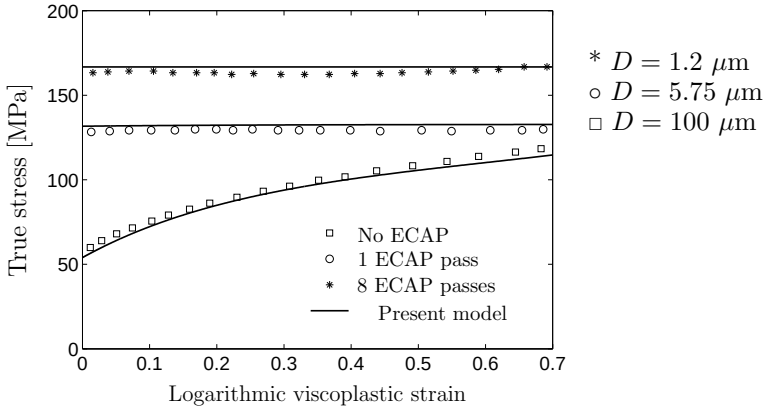

Figure 3: The present model (lines) is shown as calibrated against experimental data (symbols) for axisymmetric compression tests on AA1050 aluminum after different numbers of ECAP passes, taken from [38].

2.3 Rate sensitivity

Turning next to the rate dependence of the model, experimental evidence indicate that the rate dependence of the material is influenced by the grain size. While a coarse grain structure leaves the material virtually rate independent, a finer grain structure leads to a higher rate sensitivity. The dependence of the rate sensitivity on the average grain size has been observed in nickel by [14], in gold by [15] and in aluminum by [16, 49] and is further substantiated by the experimental results presented in [17, 50]. The influence of the grain size on the macroscopic rate sensitivity of the material is by some authors considered to be an effect of increased interaction between mobile dislocations in the grain interiors and

dislocations pinned in the grain boundaries. This is discussed concerning copper in [51, 52] and regarding nickel in [53]. A compilation of the rate dependence of the initial yield stress $\sigma_{\mathrm{y}0}$ of a 99.5%-purity aluminum, as given by [17], is shown in Fig. 4.

Fig. 4 clearly indicates a dependency of the initial yield stress on the grain size. A viscoplastic formulation is adopted where the viscoplastic strain rate is defined as

$$\dot{\varepsilon}_{\mathrm{eff}}^{\mathrm{vp}} = \frac{1}{\eta} h(\sigma_{\mathrm{eff}}, \rho_{\mathrm{d}}, D) \tag{9}$$

where η is a viscosity parameter and h an over-stress function, as originally proposed in [54]. In addition, the von Mises effective stress is defined as $\sigma_{\mathrm{eff}} = \sqrt{3J_2}$ where $J_2 = \frac{1}{2}\mathrm{tr}\left(\boldsymbol{\tau}^{\mathrm{dev}}\boldsymbol{\tau}^{\mathrm{dev}}\right)$, with $\mathrm{tr}(\cdot)$ denoting the trace of a tensorial quantity. In the present model, an over-stress function of power-law type is assumed according to

$$h = \left\langle \frac{\sigma_{\mathrm{eff}} - \sigma_{\mathrm{y}}}{\sigma_{\mathrm{y}0} + k_{\mathrm{D}}\left(\sqrt{\frac{D_0}{D}} - 1\right)} \right\rangle^{m(D)} \tag{10}$$

where $m(D)$ is a parameter controlling the rate-sensitivity of the model and σ_{y} is the yield stress defined in (6). To allow calibration against experimental data, the m-parameter is allowed to depend on the grain size according to

$$m\left(D\right) = 1 + m_1 \exp\left[m_2\left(1 - \frac{D}{D_0}\right)\right] \tag{11}$$

where m_1 and m_2 are constitutive parameters. It is noted that taking advantage of (9) and (10), a dynamic yield function [55] – indicated by a superscript d – can be established according to

$$f^{\mathrm{d}} = \sigma_{\mathrm{eff}} - \sigma_{\mathrm{y}}^{\mathrm{d}}\left(D, \dot{\varepsilon}_{\mathrm{eff}}^{\mathrm{vp}}\right) - H\left(\sqrt{\rho_{\mathrm{d}}/\rho_{\mathrm{d}}^0} - 1\right) \tag{12}$$

where the rate-dependence of the model becomes clear through the dynamic yield stress being defined as

$$\sigma_{\mathrm{y}}^{\mathrm{d}}\left(D, \dot{\varepsilon}_{\mathrm{eff}}^{\mathrm{vp}}\right) = \left[\sigma_{\mathrm{y}0} + k_{\mathrm{D}}\left(\sqrt{\frac{D_0}{D}} - 1\right)\right]\left[1 + \left(\eta\dot{\varepsilon}_{\mathrm{eff}}^{\mathrm{vp}}\right)^{1/m(D)}\right] \tag{13}$$

This dynamic yield stress is used in the calibration procedure. Note that k_{D} is already calibrated. Recalling the over-stress formulation (10), it is found that the saturation time can be held constant at $\eta = 4 \times 10^{-4}$ s while $m(D)$ varies with the grain size. The results from the calibration, showing the dependency of the dynamic yield stress on the viscoplastic strain rate for different grain sizes, are shown in Fig. 4. This calibration is obtained through the choices $m_1 = 0.0014$ and $m_2 = 8.5$ rendering a model where the rate sensitivity gradually weakens as the grain size increases, i.e. as m approaches 1.

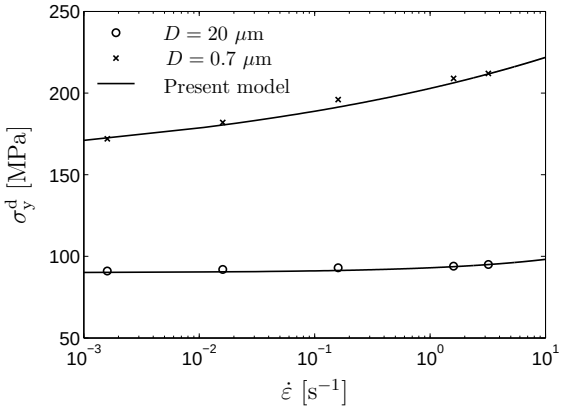

Figure 4: Variation of the macroscopic dynamic yield stress with strain rate for different grain sizes D. The present model is calibrated against the results of [17] on 99.5% purity aluminum. Note the logarithmic scale on the horizontal axis.

3 Simulation results

The microstructural variables previously introduced are now incorporated into a finite strain viscoplastic constitutive model. The kinematics are based on a multiplicative split of the deformation gradient $\boldsymbol{F}$ into $\boldsymbol{F} = \boldsymbol{F}^{\mathrm{e}}\boldsymbol{F}^{\mathrm{vp}}$, i.e. into an elastic and a viscoplastic part. The elasticity in the model is based on a simple strain energy function chosen as

$$W = K\frac{1}{2}\ln\left(J^{\mathrm{e}}\right)^2 + 2GJ_2^{\mathrm{e}} \tag{14}$$

where $J^e = \det(\boldsymbol{F}^e)$. Letting $\boldsymbol{b}^{\mathrm{e}} = \boldsymbol{F}^{\mathrm{e}}\boldsymbol{F}^{\mathrm{eT}}$ and $\boldsymbol{V}^{\mathrm{e}} = \sqrt{\boldsymbol{b}^{\mathrm{e}}}$ denote the left Cauchy-Green tensor and the left stretch tensor, respectively, the quantity $J_2^{\mathrm{e}} = \frac{1}{2}\left(\ln \boldsymbol{V}^{\mathrm{e}}\right)^{\mathrm{dev}} : \left(\ln \boldsymbol{V}^{\mathrm{e}}\right)^{\mathrm{dev}}$ was introduced in (14). The strain energy function (14) gives the Kirchhoff stress tensor according to

$$\boldsymbol{\tau} = 2\boldsymbol{b}^{\mathrm{e}}\frac{\partial W}{\partial \boldsymbol{b}^{\mathrm{e}}} = K\ln(J^{\mathrm{e}})\mathbf{1} + 2G\ln(\boldsymbol{V}^{\mathrm{e}}) \tag{15}$$

where $\mathbf{1}$ is the second-order identity tensor. The elastic constitutive parameters K and G correspond in the limit of small strains to the bulk and shear modulus, respectively. Considering aluminum, these parameters are chosen as $K = 56$ GPa and $G = 27$ GPa in the present calibration. Turning next to the inelastic behavior of the model, the evolution law for the viscoplastic part is, by adopting J_2-plasticity, given by

$$\boldsymbol{d}^{\mathrm{vp}} = \dot{\varepsilon}_{\mathrm{eff}}^{\mathrm{vp}}\frac{3}{2}\frac{\boldsymbol{\tau}_{\mathrm{r}}^{\mathrm{dev}}}{\sigma_{\mathrm{eff}}} \tag{16}$$

where $\boldsymbol{d}^{\mathrm{vp}} = \mathrm{sym}(\dot{\boldsymbol{F}}^{\mathrm{vp}}\boldsymbol{F}^{\mathrm{vp}-1})$ is the viscoplastic rate of deformation and $\boldsymbol{\tau}_{\mathrm{r}}^{\mathrm{dev}} = \boldsymbol{R}^{\mathrm{eT}}\boldsymbol{\tau}^{\mathrm{dev}}\boldsymbol{R}^{\mathrm{e}}$ the elastically rotated deviatoric Kirchhoff stress, cf. [56]. The material is the same as

Table 2: Material parameters entering the present model.

Parameter	Value	Description
d_1	715.5	Parameter controlling the creation of dislocations
d_2	7.7	Parameter controlling the annihilation of dislocations
d_3	437.5	Parameter controlling the influence of grain size on the dislocation density
k_{X}	3.8	Coefficient in the grain size evolution law
c_{X}	2	Exponent controlling how rapidly the recrystallization proceeds
k_{D}	6.8 MPa	Stress intensity factor in the Hall-Petch relation
D_0	100 μm	Initial average grain size
D_{f}	1 μm	Final average grain size
ρ_{d}^0	8×10^9 m^{-2}	Initial dislocations density
$\varepsilon_{\mathrm{c}}^{\mathrm{vp}}$	0.1	Critical viscoplastic strain at which recrystallization is initiated
η	4×10^{-4} s	Viscosity parameter in the over-stress formulation
m_1	0.0014	Parameter controlling the grain size dependent rate sensitivity
m_2	8.5	Parameter controlling the grain size dependent rate sensitivity
σ_{y0}	48.6 MPa	Initial yield stress
K	56 GPa	Bulk modulus
G	27 GPa	Shear modulus
H	0.7 MPa	Isotropic hardening modulus

that the model was calibrated to. Table 2 summarizes the material parameters entering the present formulation The model was implemented as a user subroutine into the finite element code Abaqus Explicit. For the integration of the constitutive laws a fully implicit integration based on an Euler backward scheme was utilized. Note that beside the evolution equations for the dislocation density and the grain size, only one additional scalar equation related to the effective viscoplastic strain enters the local stress-updating algorithm, rendering a numerically efficient implementation of the model. These aspects are discussed in [57].

The ECAP process, illustrated in Fig. 1, is studied for different geometrical configurations defined by $\Phi = 90^\circ$ and $\Phi = 120^\circ$. The die angle is in both cases $\Psi = 20^\circ$. It is expected that $\Phi = 90^\circ$ will result in a nearly homogeneous microstructure in terms of grain size and dislocation density whereas for $\Phi = 120^\circ$, a more inhomogeneous microstructure is expected. The radius of the inner corner of the die is set to $0.1w$ and the billet width is set to $w = 20$ mm.

Plane strain conditions are assumed in the analysis and the size of the specimen is $20 \times 20 \times 150$ mm. For the finite element calculations the mesh is defined by 20×150 four-node elements based on reduced integration. This mesh discretization is based on the observations done by [58] that 20 elements along the billet width is required to capture the distribution of equivalent plastic strain. The simulations are displacement controlled and by specifying a given velocity of 50 mm/s to a flat rigid tool the specimen is pressed into the die. It is assumed that Coulomb friction exist between the die and the workpiece with a friction coefficient of 0.02. As plane strain conditions are assumed it allows for the simulation of route C with two consecutive stages, i.e. with a 180° rotation of the specimen in between the passes. This is achieved by using two tools and a die channel with two bends. The first tool is pressing the specimen through the first ECAP pass after which

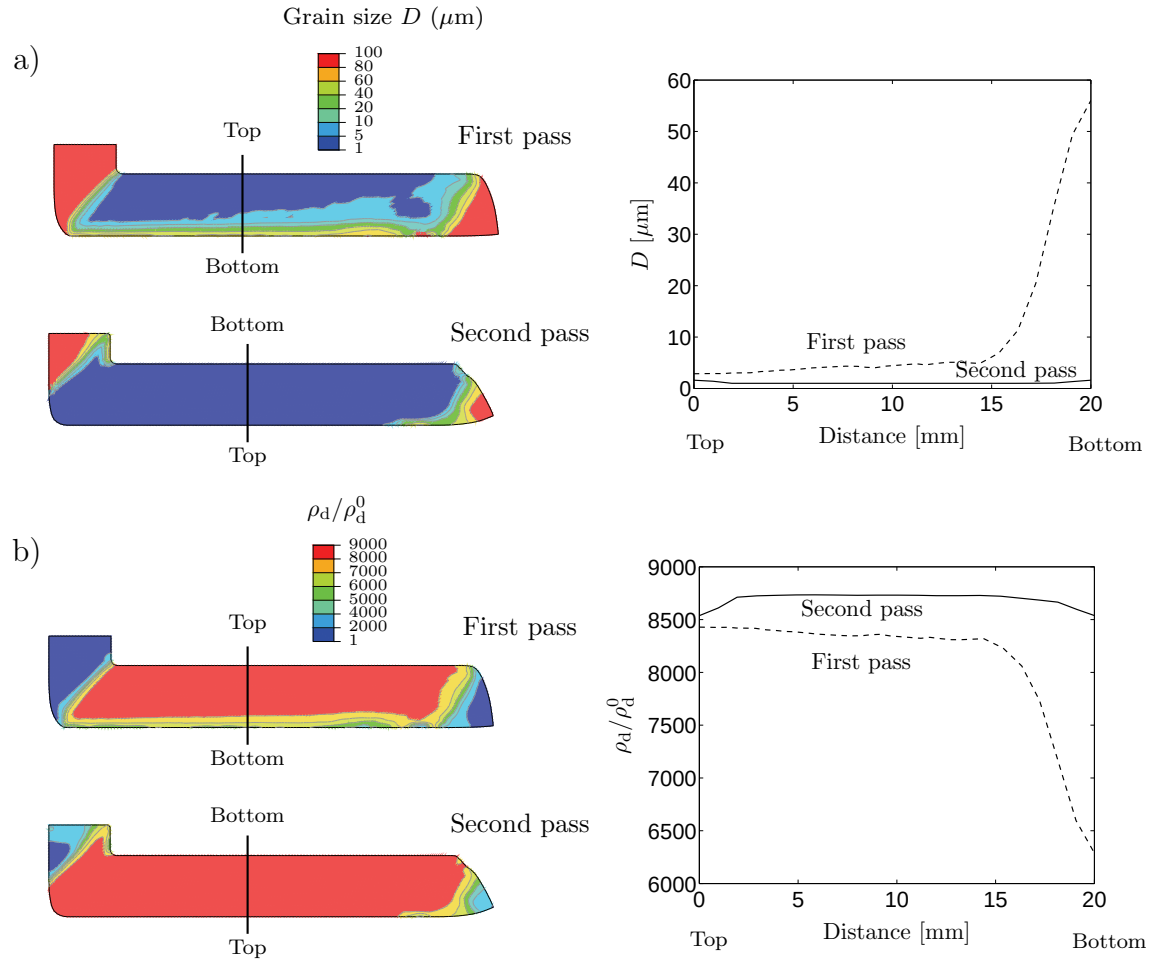

Figure 5: Results for route C with two passes are shown, note that the specimen is rotated 180° before the second pass. a) Grain size and b) dislocation density distributions for the ECAP geometry $\Psi = 20°$ and $\Phi = 90°$. The graphs to the right show the variation of grain size and dislocation density in the section indicated in the left plots.

a second tool is activated, pressing the specimen though the second ECAP pass. The die geometry used is essentially the same as in [59], but with the modifications that two tools are used and that the specimen does not enter the second ECAP pass before the first pass is finished.

Consider first the geometry defined by $\Phi = 90°$ and $\Psi = 20°$. The results from the simulations are shown in Fig. 5, where both the grain size as well as the dislocation density are shown. Note that in the second pass, as the specimen is rotated 180°, the reference sides, denoted by Top and Bottom, are interchanged. During the first pass, an initial transition part exists at the front of the specimen but behind this section a steady state region is obtained. The simulations show that after one pass neither the grain size nor the

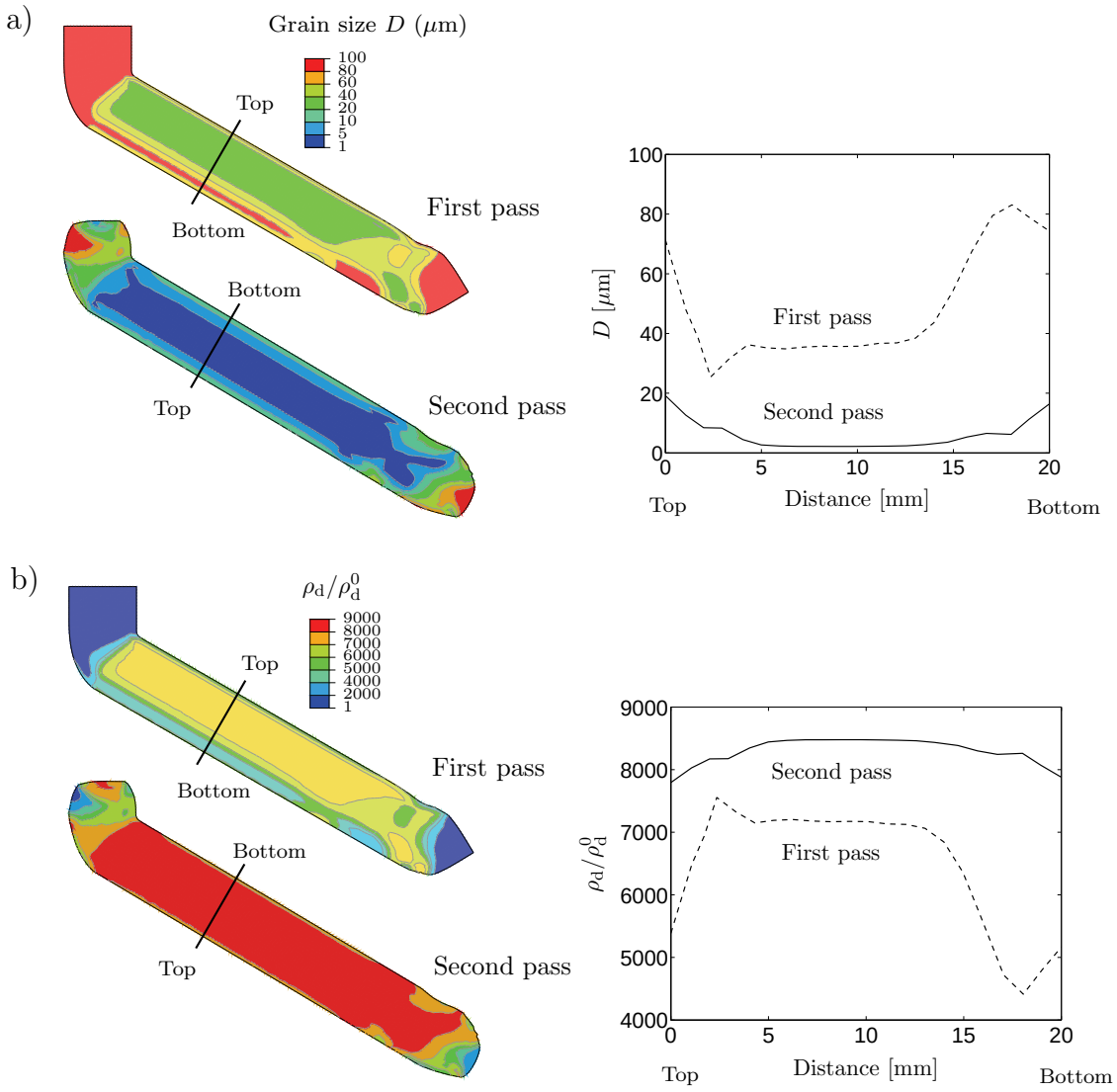

Figure 6: Results for route C with two passes are shown, note that the specimen is rotated 180° before the second pass. a) Grain size and b) dislocation density distributions for ECAP geometry $\Psi = 20°$ and $\Phi = 120°$. The graphs to the right show the variation of grain size and dislocation density in the section indicated in the left plots.

dislocation density are homogeneously distributed in the specimen. The largest deviations from a homogeneous state are found at the bottom part of the specimen stretching about one fourth into the specimen. This is clearly seen in the plots shown in Fig. 5.

After the second pass, ignoring the transition region, an almost homogeneous distribution of grain size and dislocation density is found. The grain size, D, in a cross section varies between 1 μm and 1.6 μm and the normalized dislocation density, ρ_d/ρ_d^0, between

8500 and 8700.

Metallographic studies on 1050 aluminum, ECAP-processed at different temperatures, is presented by e.g. [16] and corresponding results from experiments conducted at room temperature by e.g. [41, 60, 61]. It should be noted, however, that the ECAP:ed specimens used in these studies are annealed before the metallographic study, making a direct comparison with the results in Figs. 5 and 6 difficult.

The results from the ECAP geometry defined by $\Phi = 120^\circ$ and $\Psi = 20^\circ$ are shown in Fig. 6. Through a comparison with the results for the ECAP geometry defined by $\Phi = 90^\circ$ and $\Psi = 20^\circ$ it is clear that a more inhomogeneous distribution of grain size and dislocation density is obtained. This holds for both the first as well as for the second ECAP pass. Results from the first pass reveal that large deviations from a homogeneous state are found both at the top and at the bottom of the specimen. After the second pass these deviations are less obvious but they are, however, still present as seen in the plots in Fig. 6. In a cross section, the grain size, D, varies between 4 μm and 20 μm and the normalized dislocation density, $\rho_{\mathrm{d}}/\rho_{\mathrm{d}}^0$, between 5100 and 7500.

4 Concluding remarks

Considering micromechanical processes such as the multiplication, interaction and annihilation of dislocations as well as the influence of continuous dynamic recrystallization, a micromechanically motivated constitutive model is formulated. The model recognizes the influence of grain size on the material behavior at both the macro- and the microlevel. The macroscopic yield stress is influenced by the grain size through a component corresponding to the Hall-Petch relation. In addition, considering experimental evidence, the macroscopic rate dependence of the model is allowed to depend on the grain size. On the microlevel, recrystallization influences the evolution of the dislocation density since an increased amount of grain boundary area restricts the movement of mobile dislocations and since the recrystallization involves the formation of new, relatively dislocation-free, grains. By calibration of the model against experimental findings – as is shown – a micromechanically motivated and versatile tool for macroscale simulations of materials and conditions involving finite strain viscoplasticity and continuous dynamic recrystallization is proposed.

References

[1] S. Gourdet and F. Montheillet. An experimental study of the recrystallization mechanism during hot deformation of aluminium. *Materials Science and Engineering*, A283:274–288, 2000.

[2] M. E. Kassner and S. R. Barrabes. New developments in geometric dynamic recrystallization. *Materials Science and Engineering*, A410-411:152–155, 2005.

[3] I. Mazurina, T. Sakai, H. Miura, O. Sitdikov, and R. Kaibyshev. Effect of deformation temperature on microstructure evolution in aluminum alloy 2219 during hot ECAP. *Materials Science and Engineering*, A486:662–671, 2008.

[4] T. Sakai, H. Miura, and X. Yang. Ultrafine grain formation in face centered cubic metals during severe plastic deformation. *Materials Science and Engineering*, A499:2–6, 2009.

[5] R. O. Kaibyshev, I. A. Mazurina, and D. A. Gromov. Mechanisms of grain refinement in aluminum alloys in the process of severe plastic deformation. *Metal Science and Heat Treatment*, 48(1-2):57–62, 2006.

[6] C. Liu, S. Jiang, and X. Zhang. Continuous dynamic recrystallization and discontinuous dynamic recrystallization in 99.99% polycrystalline aluminum during hot compression. *Transactions of Nonferrous Metals Society of China*, 15(1):82–86, February 2005.

[7] H. Yamagata, Y. Ohuchida, N. Saito, and M. Otsuka. Nucleation of new grains during discontinuous dynamic recrystallization of 99.998 mass% Aluminum at 453K. *Scripta Materialia*, 45:1055–1061, 2001.

[8] W. Q. Cao, A. Godfrey, W. Liu, and Q. Liu. Annealing behavior of aluminium deformed by equal channel angular pressing. *Materials Letters*, 57:3767–3774, 2003.

[9] S. Gourdet and F. Montheillet. A model of continuous dynamic recrystallization. *Acta Materialia*, 51:2685–2699, 2003.

[10] U. F. Kocks. Laws for Work-Hardening and Low-Temperature Creep. *Journal of Engineering Materials and Technology*, 98(1):76–85, January 1976.

[11] H. Mecking and U. F. Kocks. Kinetics of flow and strain-hardening. *Acta Metallurgica*, 29:1865–1875, 1981.

[12] G. Z. Voyiadjis and F. H. Abed. Microstructural based models for bcc and fcc metals with temperature and strain rate dependency. *Mechanics of Materials*, 37:355–378, 2005.

[13] Y. Estrin and H. S. Kim. Modelling microstructure evolution toward ultrafine crystallinity produced by severe plastic deformation. *Journal of Materials Science*, 42:1512–1516, 2007.

[14] R. Schwaiger, B. Moser, M. Dao, N. Chollacoop, and S. Suresh. Some critical experiments on the strain-rate sensitivity of nanocrystalline nickel. *Acta Materialia*, 51:5159–5172, 2003.

[15] R. D. Emery and G. L. Povirk. Tensile behavior of free-standing gold films. Part II. Fine-grained films. *Acta Materialia*, 51:2079–2987, 2003.

[16] J. May, H. W. Höppel, and M. Göken. Strain rate sensitivity of ultrafine-grained aluminum processed by severe plastic deformation. *Scripta Materialia*, 53:189–194, 2005.

[17] H. Miyamoto, K. Ota, and T. Mimaki. Viscous nature of deformation of ultra-fine grain aluminum processed by equal-channel angular pressing. *Scripta Materalia*, 54:1721–1725, 2006.

[18] Y. Estrin and H. Mecking. A unified phenomenological description of work hardening and creep based on one-parameter models. *Acta Metallurgica*, 32(1):57–70, 1984.

[19] F. J. Humphreys and M. Hatherly. *Recrystallization and related annealing phenomena*. Pergamon, New York, second edition, 1996.

[20] D. A. Molodov, P. Konijnenberg, W. Hu, G. Gottstein, and L. S. Shvindlerman. Effect of dislocation absorption on the motion of specific grain boundaries in Al-bicrystals. *Acta Materialia*, 45:229–235, 2001.

[21] J. T. M. De Hosson, W. A. Soer, A. M. Minor, Z. Shan, E. A. Stach, S. A. S. Asif, and O. L. Warren. In situ TEM nanoindentation and dislocation-grain boundary interactions: a tribute to David Brandon. *Journal of Materials Science*, 41:7704–7719, 2006.

[22] V. M. Segal, V. I. Reznikov, A. E. Drobyshevskiy, and V. I. Kopylov. Plastic working of metals by simple shear. *Russian Metallurgy*, 1:99–105, 1981.

[23] R. Z. Valiev and T. G. Langdon. Principles of equal-channel angular pressing as a processing tool for grain refinement. *Progress in Materials Science*, 51:881–981, 2006.

[24] T. G. Langdon. The principles of grain refinement in equal-channel angular pressing. *Materials Science and Engineering*, A462:3–11, 2007.

[25] Y. Iwahashi, J. Wang, Z. Horita, and M. Nemoto. Principles of equal-channel angular pressing for the processing of ultra-fine grained materials. *Scripta Materialia*, 35(2):143–146, 1996.

[26] H. K. Kim and W. J. Kim. Microstructural instability and strength of an AZ31Mg alloy after severe plastic deformation. *Materials Science and Engineering*, A385:300–308, 2004.

[27] A. P. Zhilyaev, K. Oh-ishi, G. I. Raab, and T. R. McNelley. Influence of ECAP processing parameters on texture and microstructure of commercially pure aluminum. *Materials Science and Engineering*, A441:245–252, 2006.

[28] W. Skrotzki, N. Scheerbaum, C.-G. Oertel, H.-G. Brokmeier, S. Suwas, and L. S. Tóth. Recrystallization of high-purity aluminum during equal channel angular pressing. *Acta Materialia*, 55:2211–2218, 2007.

[29] R. D. Doherty, D. A. Hughes, F. J. Huphreys, J. J. Jonas, D. Juul Jensen, M. E. Kassner, W. E. King, T. R. McNelley, H. J. McQueen, and A. D. Rollett. Current issues in recrystallization: a review. *Materials Science and Engineering A*, 238:219–274, 1997.

[30] B. Derby. The dependence of grain size on stress during dynamic recrystallization. *Acta Metallurgica et Materialia*, 39(5):955–962, 1991.

[31] B. Derby. Dynamic recrystallization: The steady state grain size. *Scripta Metallurgica et Materialia*, 27:1581–1586, 1992.

[32] E. P. Busso. A continuum theory for dynamic recrystallization with microstructure-related length scales. *International Journal of Plasticity*, 14(4-5):319–353, 1998.

[33] E. Cerri, E. Evangelista, A. Forcellese, and H. J. McQueen. Comparative hot workability of 7012 and 7075 alloys after different pretreatments. *Materials Science and Engineering*, A197:181–198, 1995.

[34] S. L. Semiatin, P. B. Berbon, and T. G. Langdon. Deformation heating and its effect on grain size evolution during equal channel angular extrusion. *Scripta Materialia*, 44:135–140, 2001.

[35] M. Cabibbo, E. Evangelista, and V. Latini. Thermal stability study on two aluminum alloys processed with equal channel angular pressing. *Journal of Materials Science*, 39:5659–5667, 2004.

[36] Y. G. Kim, B. Hwang, S. Lee, W. G. Kim, and D. H. Shin. Dynamic deformation and fracture behavior of ultrafine-grained aluminum alloy fabricates by equal-channel angular pressing. *Metallurgical and Materials Transactions A*, 36A:2947–2955, November 2005.

[37] D. G. Morris and M.A. Muños-Morris. Microstructure of severely deformed Al-3Mg and its evolution during annealing. *Acta Materialia*, 50:4047–4060, 2002.

[38] S. Poortmans and B. Verlinden. Mechanical properties of fine-grained AA1050 after ECAP. *Materials Science Forum*, 503-504:847–852, 2000.

[39] H. J. McQueen and J. E. Hockett. Microstructures of Aluminum compressed at various rates and temperatures. *Metallurgical Transactions*, 1:2997–3004, November 1970.

[40] N. S. Ottosen and M. Ristinmaa. *The Mechanics of Constitutive Modeling*. Elsevier, first edition, 2005.

[41] E. A. El-Danaf, M. S. Soliman, A. A. Almajid, and M. M. El-Rayes. Enhancement of mechanical properties and grain size refinement of commercial purity aluminum 1050 processed by ECAP. *Materials Science and Engineering*, A458:226–234, 2007.

[42] E. Kovács-Csetényi, M. Horváth, N. Q. Chinh, and I. Kovács. Effect of grain size on tensile stress and ductility in Al99.99. *Physica Status Solidi*, A166:805–810, 1998.

[43] H. Hasegawa, S. Komura, A. Utsunomiya, Z. Horita, M. Furukawa, M. Nemoto, and T. G. Langdon. Thermal stability of ultrafine-grained aluminum in the presence of Mg and Zr additions. *Materials Science and Engineering*, A265:188–196, 1999.

[44] I. Kovács, N. Q. Chinh, and E. Kovács-Csetényi. Grain size dependence of the work hardening process in Al99.99. *Physica Status Solidi*, A194(1):3–18, 2002.

[45] Y. Estrin. Dislocation theory based constitutive modelling: foundations and applications. *Journal of Materials Processing Technology*, 80-81:33–39, 1998.

[46] L. Capolungo. *Modeling of the size effect in the plastic behavior of polycrystalline materials*. PhD thesis, Georgia Institute of Technology, 2007.

[47] L. Barbé. *Physical Metallurgy of P-alloyed TRIP Steels*. PhD thesis, University of Gent, 2006.

[48] N. Q. Chinh, G. Hrováth, Z. Horita, and T. G. Langdon. A new constitutive relationship for the homogeneous deformation of metals over a wide range of strain. *Acta Materialia*, 52:3555–3563, 2004.

[49] J. May, D. Amberger, M. Dinkel, H. W. Höppel, and M. Göken. Monotonic and cyclic deformation behaviour of ultrafine-grained aluminium. *Materials Science and Engineering*, A483-484:481–484, 2008.

[50] Q. Wei, S. Cheng, K. T. Ramesh, and E. Ma. Effect of nanocrystalline and ultrafine grain sizes on the strain rate sensitivity and activation volume: fcc versus bcc metals. *Materials Science and Engineering*, A381:71–79, 2004.

[51] F. H. Dalla Torre, E. V. Pereloma, and C. H. J. Davies. Strain hardening behaviour and deformation kinetics of Cu deformed by equal channel angular extrusion from 1 to 16 passes. *Acta Materialia*, 54:1135–1146, 2006.

[52] Y. J. Li, X. H. Zeng, and W. Blum. Transition from strengthening to softening by grain boundaries in ultrafine-grained Cu. *Acta Materialia*, 52:5009–5018, 2004.

[53] L. Hollang, E. Hieckmann, D. Brunner, C. Holste, and W. Skrotzki. Scaling effects in the plasticity of nickel. *Materials Science and Engineering*, A424:138–153, 2006.

[54] P. Perzyna. Fundamental problems in viscoplasticity. *Advances in Applied Mechanics*, 9:243–377, 1966.

[55] M. Ristinmaa and N. S. Ottosen. Consequences of dynamic yield surface in viscoplasticity. *International Journal of Solids and Structures*, 37:4601–4622, 2000.

[56] M. Wallin and M. Ristinmaa. Deformation gradient based kinematic hardening model. *International Journal of Plasticity*, 21:2025–2050, 2005.

[57] H. Hallberg, K. Ryttberg, and M. Ristinmaa. Model describing material-dependent deformation behavior in high velocity metal forming processes. *ASCE Journal of Engineering Mechanics*, 135(4):345–357, 2009.

[58] S. Li, M. A. M. Bourke, I. J. Beyerlein, D. J. Alexander, and B. Clausen. Finite element analysis of the plastic deformation zone and working load in equal channel angular extrusion. *Materials Science and Engineering*, A382:217–236, 2004.

[59] H. S. Kim. Finite element analysis of deformation behaviour of metals during equal channel multi-angular pressing. *Materials Science and Engineering*, A328:317–322, 2002.

[60] W. Q. Cao, A. Godfrey, and Q. Liu. EBSP investigation of microstructure and texture evolution during equal channel angular pressing of aluminium. *Materials Science and Engineering*, A361:9–14, 2003.

[61] X. G. Qiao, M. J. Starink, and N. Gao. Hardness inhomogeneity and local strengthening mechanisms of an Al1050 aluminium alloy after one pass of equal channel angular pressing. *Materials Science and Engineering*, A513-514:52–58, 2009.